33rd Annual International Conference of the IEEE EMBS
Boston, Massachusetts USA, August 30 - September 3, 2011

Portable and Cost-effective Pixel Super-Resolution On-Chip Microscope for Telemedicine Applications

Waheb Bishara, Uzair Sikora, Onur Mudanyali, Ting-Wei Su, Oguzhan Yaglidere, Shirley Luckhart, and Aydogan Ozcan, *Senior Member, IEEE*

***Abstract*— We report a field-portable lensless on-chip microscope with a lateral resolution of <1μm and a large field-of-view of ~24mm^2. This microscope is based on digital in-line holography and a pixel super-resolution algorithm to process multiple lensfree holograms and obtain a single high-resolution hologram. In its compact and cost-effective design, we utilize 23 light emitting diodes butt-coupled to 23 multi-mode optical fibers, and a simple optical filter, with no moving parts. Weighing only ~95 grams, we demonstrate the performance of this field-portable microscope by imaging various objects including human malaria parasites in thin blood smears.**

I. Introduction

OPTICAL microscopy is an indispensable tool in science and medicine, despite the plethora of imaging and detection techniques currently available. Optical microscopy is used for blood tests, disease diagnostics, and water quality assessment, among many other uses, and is essential in many scientific laboratories. For certain application and conditions, such as infectious disease diagnostics or water quality monitoring in resource poor conditions or field settings, device specifications such as low weight, compactness and robustness may become more important than specifications considered in an advanced research laboratory.

Along those lines, several efforts in recent years have been aimed at providing microscopes suitable for addressing global health issues under field-use conditions [1-4]. With these same goals in mind, we report in this work a portable lensless microscope which is based on in-line holography and pixel super-resolution. This microscope achieves a spatial resolution of <1μm over a large field-of-view (FOV) of ~24mm^2. It is composed of inexpensive components, contains no lenses or moving parts, and weighs ~95 grams (see Fig. 1). As a demonstration of the practicality of this microscope, we report using this device to image human malaria parasites (*Plasmodium falciparum*) in thin blood smears, in both amplitude and phase channels.

Manuscript received March 26, 2011.

W. Bishara*, U. Sikora, O. Mudanyali, T. W. Su, O. Yaglidere, and A. Ozcan are with Department of Electrical Engineering, University of California, Los Angeles, 90095, USA (*email: bishara@ucla.edu, Tel: 310-206-2050).

S. Luckhart is with the Department of Microbiology and Immunology, University of California, Davis, CA, 95616, USA.

A. Ozcan is also with the California NanoSystems Institute, University of California, Los Angeles, CA, 90095, USA (email: ozcan@ucla.edu, http://innovate.ee.ucla.edu/).

II. Principles of Operation

Our lensless microscope utilizes simple and inexpensive light-emitting diodes (LEDs) and optical fibers in a particular configuration (Fig. 1) which allows formation of holograms of the objects to be imaged despite the limited spatial and temporal coherence of the illumination source [3-5]. In our microscope, multiple lensless holograms which are spatially shifted with respect to each other are sequentially recorded. After the lateral shifts between different holograms are digitally estimated, these lensfree holograms are input to a pixel super-resolution algorithm which yields a single high-resolution hologram, effectively having a much smaller pixel size.[5] This high-resolution hologram is then rapidly processed using an iterative phase-retrieval algorithm to generate a high-resolution complex valued microscope image of the object.[3]

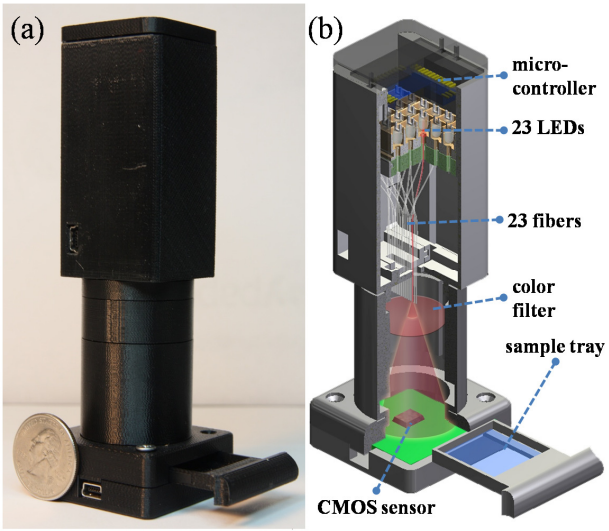

Fig. 1. A photograph and a schematic diagram of our lensless high-resolution microscope are shown. 23 LEDs are butt-coupled to 23 optical fibers, each with 105μm core size. These LEDs are turned on sequentially, one at a time, using an inexpensive micro-controller. These recorded lensfree holograms are then rapidly processed to create high-resolution images of the specimens over a large FOV of ~24mm^2.

A schematic diagram and a photograph of our microscope are shown in Fig. 1. A CMOS image sensor

with a pixel pitch of 2.2μm and a total active area of 24mm^2 is used. The sample to be imaged is placed directly above the protective glass of the CMOS sensor, i.e., at ~0.7mm away from the active area of the sensor (see Fig. 1). Approximately 5cm away from the sample is an array of 105μm core multi-mode optical fibers arranged in a line. Each optical fiber is butt-coupled (without the use of any light coupling optics or mechanical components) at its other end to an LED (λ=640nm). The illumination from the LEDs has a bandwidth of approximately 20nm, and is filtered down to ~10nm using a simple color filter. A digital microcontroller (Atmel ATmega8515, ~3USD/per piece) sequentially turns on the LEDS, one at a time, and for each LED illumination, a lensfree holographic image is recorded. The microcontroller and the CMOS sensor are connected to a computer by a USB cable and are synchronized by the accompanying software.

The large core size of the optical fibers allows easy coupling to the LEDs, while the large distance between the free ends of the fibers and the sample allows the illumination wavefronts to develop spatial coherence by the time they reach the sample plane, despite the large core of the fiber and the limited coherence of the LEDs. The hologram formed at the sensor plane is due to the interference between the light scattered from the objects and the undisturbed portion of the wavefront. As different LEDs are turned on, the same hologram is shifted parallel to the sensor plane. Due to our unique hologram recording geometry shown in Fig. 1, the shift of each lensfree hologram at the sensor plane is more than two orders of magnitude smaller than the distance between the free ends of the adjacent fibers.

A single lensless hologram captured with the 2.2μm pixel pitch at the CMOS sensor plane is undersampled, as shown in Fig. 2, left image, where spatial aliasing is visible especially at the edges of the hologram. To overcome this undersampling issue, multiple shifted holograms are processed using a pixel super-resolution algorithm [5] as emphasized earlier. Toward this end, the shifts between different holograms are initially computed directly from the raw lensfree holograms without the need to know any geometrical parameters of the system. This shift estimation is performed by a combination of cross correlation operations for the integer pixel part of the shifts and an iterative gradient-based estimation for accurate sub-pixel shift estimation. Integer pixel shifts are simply used to roughly align the captured images to each other, but add no additional information to a captured holographic scene. Sub-pixel shifts, on the other hand, allow resolving high spatial frequencies that are inaccessible from a single hologram due to spatial undersampling. Fig. 3 shows the estimated sub-pixel shifts between different holograms captured by the sensor, after discarding the integer pixel shifts which range up to 30 pixels along the direction of the fiber array.

The pixel super-resolution algorithm we implemented [5-7] takes in sub-pixel shifted images x_k, each with M pixels, and outputs a single high-resolution image $\mathbf{Y}$, on a much finer grid, which is compatible with all the shifted images. This pixel super-resolved high-resolution image is obtained by minimizing a cost function $C(\mathbf{Y})$ composed of the distance between the measured images x_k and the appropriate down-samplings of the high-resolution image, labeled $\tilde{x}_k$. An additional penalty giving weight to high frequencies in $\mathbf{Y}$ is added to suppress artifacts. In our results, we used a Laplacian filter to generate the high-frequency filtered $\mathbf{Y}_{fil}$.

$$C(\mathbf{Y}) = \frac{1}{2} \sum_{\substack{k=1,\ldots,p \\ i=1,\ldots,M}} (x_{k,i} - \tilde{x}_{k,i})^2 + \frac{\alpha}{2} (\mathbf{Y}_{fil}^T \bullet \mathbf{Y}_{fil}) \quad (1)$$

An example of the resolution enhancement of the captured hologram due to pixel super-resolution is shown in Fig. 2, right image. The raw hologram captured by the sensor is limited in spatial frequency and therefore displays aliasing apparent in the curvature of the fringes. When using the 23 shifted holograms captured by the device to generate a single higher resolution image, the fringes are clearly resolved (see Fig. 2). This translates to a higher effective numerical aperture for our microscope, and to a higher-resolution image, as will be shown below.

After a high-resolution hologram is generated, it must be processed to recover a microscope image of the object. This step requires recovering the phase of the optical field which was lost when recording the intensity at the sensor plane. We performed phase-retrieval using an iterative algorithm that utilizes the object support as a constraint in the iterations in addition to the measured intensity constraint at the sensor-array. We note that despite the well known twin-image artifacts present in the initial hologram due to the loss of phase, it is still possible to identify the support of the object imaged. This allows iterative phase retrieval and successful removal of the twin image artifact [3-5].

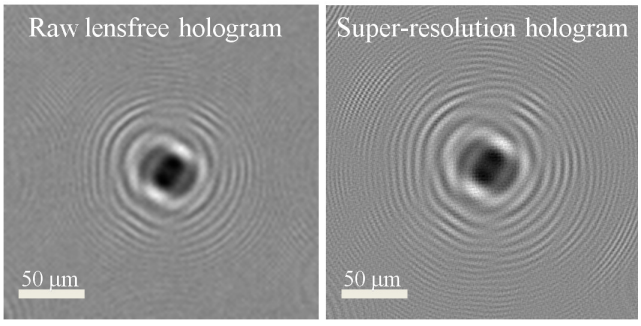

Fig. 2. Left: The raw lensfree hologram as captured by the 2.2μm sensor-array. Spatial aliasing is apparent from the direction of the fringes toward the edges. Our pixel super-resolution algorithm utilizes 23 shifted holograms to recover the higher resolution hologram shown on the right.

III. Results

To test the performance of our portable super-resolution microscope, we fabricated micron-scale patterns etched in glass using focused ion beam (FIB) milling. Ideally, these objects are phase only objects, with a phase value which depends on the depth of etching. The hologram captured by the sensor of one such pattern is shown in Fig. 2, left. As described above, 23 different lensfree holograms are captured by sequentially turning on different LEDs, one at a time. The total capture time is limited by the frame rate of the sensor, which in this case was 5 frames per second, though much faster sensors are commercially available. The pixel super-resolution algorithm yields the high resolution hologram shown in Fig. 2, right.

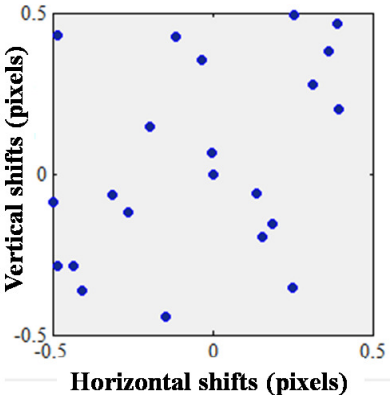

Fig. 3. Sub-pixel shifts between different ray holograms, with the first hologram as a reference, after discarding the integer pixel shifts which contain no information regarding higher resolution content of the image.

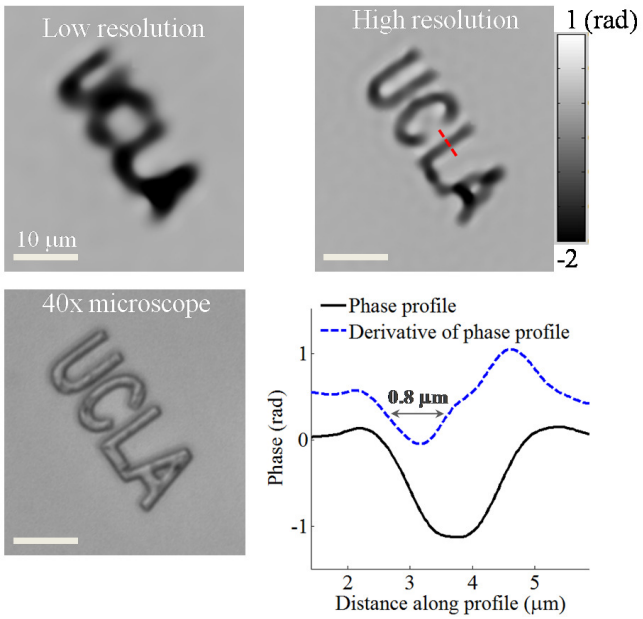

Fig. 4. Phase images of a fabricated micron-scale pattern etched in glass acquired using our super-resolution microscope, and a comparison to a bright-field microscope image. The low resolution image is the result of processing a single lensfree hologram captured by the CMOS sensor. The high resolution image is the result of processing all 23 lensfree holograms using the pixel super-resolution algorithm, and it clearly shows resolution enhancement compared to the lower resolution image. The super-resolved image compares well to the 40x objective (NA = 0.65) bright field microscope image. The phase profile along the dashed line shows a spatial resolution of < 1µm.

The resulting microscope images after executing the phase-retrieval algorithm on our lensfree holograms are shown in Fig. 4. Note that we only showed phase images in this figure as this pattern is ideally a phase only object. The low resolution microscope image is the result of processing a single lensfree hologram captured by the CMOS sensor, i.e., the hologram shown in Fig. 2, left. The high-resolution microscope phase image is the result of processing the super-resolved hologram of the same object using all 23 shifted holograms. Resolution is clearly enhanced by utilizing multiple lensfree holograms. To get an idea of the resolution of these images, we plot the phase profile and its one-dimensional derivative across the letter L, from which we conclude that the resolution is < 1µm. The gap between the letters U and C is 1µm, and it also is clearly resolved.

To demonstrate the possible uses for such a portable microscope we imaged human malaria parasites (*Plasmodium falciparum*) cultured in blood. The samples were prepared by standard thin smearing of blood on microscope cover slips and staining with Giemsa stain. The amplitude and phase images obtained using our portable microscope are shown in Fig. 5, along with bright-field microscope images for comparison.

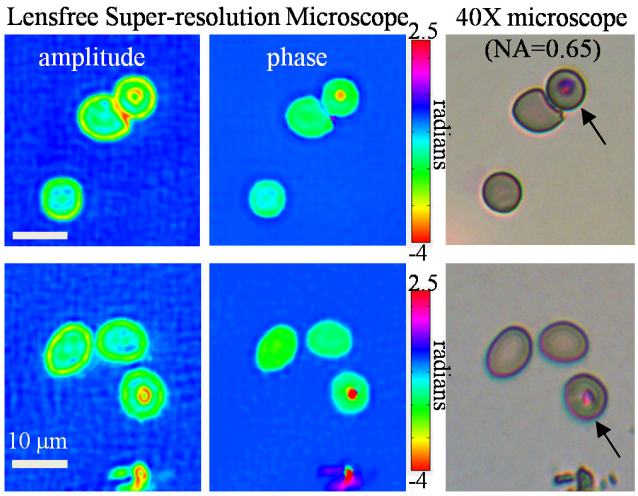

Fig. 2. Imaging of malaria parasites in a standard Giemsa stained thin blood smear. Amplitude and phase images obtained using our field-portable lensless super-resolution microscope clearly show the parasites within the red blood cells. Bright-field microscope images captured with a 40x objective lens (NA = 0.65) are also shown for comparison purposes. The infected blood cells are marked with arrows.

The combination of phase and amplitude images obtained from the lensless super-resolution microscope allows distinguishing between infected and healthy blood cells, as can be seen in Fig. 5. We should also note that the FOV of this lensless microscope is 24mm^2 without any noticeable aberration across the entire FOV [5], which is approximately two orders of magnitude larger than the FOV of a typical bright-field 40x objective lens. This allows capturing a

statistically significant number of blood cells within a single FOV. The standard procedure for malaria blood testing using a conventional lens-based microscope involves capturing multiple fields-of-view in order to overcome statistical variations due to the small number of cells in a single FOV. We hope that these results constitute a first step toward using our lensless on-chip microscope for fully automated diagnosis of malaria.

ACKNOWLEDGMENT

A. Ozcan gratefully acknowledges the support of NSF CAREER Award, the ONR Young Investigator Award and the NIH Director's New Innovator Award DP2OD006427 from the Office of The Director, NIH. The authors also acknowledge the support of the Gates Foundation, Vodafone Americas Foundation, and NSF BISH program (under Awards # 0754880 and 0930501). The authors also acknowledge Derek Tseng of UCLA for his assistance with the figures, and Kong Wai Cheung of UC Davis for maintenance of *Plasmodium falciparum* cultures and for his assistance with preparation of thin smears of infected red blood cells.

REFERENCES

[1] A.R. Miller, G.L. Davis, Z.M. Oden, M.R. Razavi, A. Fateh, M. Ghazanfari, F. Abdolrahimi, S. Poorazar, F. Sakhaie, R.J. Olsen, A.R. Bahrmand, M.C. Pierce, E.A. Graviss, and R. Richards-Kortum, "Portable, battery-operated, low-cost, bright field and fluorescence microscope," PloS One, vol. **5**, 2010, p. e11890.

[2] D.N. Breslauer, R.N. Maamari, N.A. Switz, W.A. Lam, and D.A. Fletcher, "Mobile Phone Based Clinical Microscopy for Global Health Applications," PLoS ONE, vol. **4**, 2009, p. e6320.

[3] O. Mudanyali, D. Tseng, C. Oh, S.O. Isikman, I. Sencan, W. Bishara, C. Oztoprak, S. Seo, B. Khademhosseini, and A. Ozcan, "Compact, light-weight and cost-effective microscope based on lensless incoherent holography for telemedicine applications," Lab on a Chip, vol. **10**, 2010, p. 1417.

[4] D. Tseng, O. Mudanyali, C. Oztoprak, S.O. Isikman, I. Sencan, O. Yaglidere, and A. Ozcan, "Lensfree microscopy on a cellphone," Lab on a Chip, vol. **10**, 2010, p. 1787.

[5] W. Bishara, T.-W. Su, A.F. Coskun, and A. Ozcan, "Lensfree on-chip microscopy over a wide field-of-view using pixel super-resolution," Optics Express, vol. **18**, 2010, p. 11181.

[6] R.C. Hardie, "High-resolution image reconstruction from a sequence of rotated and translated frames and its application to an infrared imaging system," Optical Engineering, vol. **37**, 1998, p. 247.

[7] Sung Cheol Park, "Super-resolution image reconstruction: a technical overview," IEEE Signal Processing Magazine, vol. **20**, 2003, pp. 21-36.